Vietnam Journal of CHEMISTRY

INSTITUTE OF CHEMISTRY,
VIETNAM ACADEMY OF SCIENCE AND TECHNOLOGY

Research Article
Free Access

Hydrazineylidene-3-oxopropanal derivatives as antiviral agents for treatment of HBV and HCV:

Experimental, DFT, and molecular docking studies

Innocent Benjamin, Hitler Louis, Akaninyene D. Udoikono, Ernest C. Agwamba, Tomsmith O. Unimuke, Eze F. Ahuekwe
First published: 27 January 2023

https://doi.org/10.1002/vjch.202200063
Citations: 1

Abstract

In this study, two derivatives of hydrazineylidene-3-oxopropanal: chlorophenyl (CPHO) and Nitrophenyl (NPHO) substituted hydrazineylidene compounds were synthesized, spectroscopically characterized using (FT-IR, UV, and NMR), and theoretically modelled as a potential drug for the treatment of antiviral hepatitis (HBV and HCV) using *in-sillico* molecular docking approach. Electronic structure investigation based on density functional theory (DFT) at the B3LYP/6-311++G(d,p) level of theory was conducted for the investigation of the structural, reactivities, and electronic properties of the studied compounds. The FT-IR analysis in gas, water, ethanol and DMSO indicates a maximum stretching vibrations frequencies of C-H in NPHO between 3249.38 to 3254.77 cm^{-1} and 3236.04 to 3240.66 cm^{-1} for CPHO, N-H for NPHO is 3309.81 to 3336.37 cm^{-1}, and CPHO is 3330.11 to 3331.18 cm^{-1}, C=O in NPHO to be 1685.55 to 1705.60 cm^{-1}, and 1700.31 to 1679.15 cm^{-1} for CPHO. The C-N stretching vibrations in NPHO were 1519.98 to 1562.06 cm^{-1} and 1430.05 to 1460.33 cm^{-1} for CPHO. The UV-Vis analysis indicates that NPHO wavelength absorption spectrum showed high excitation energy bands between 369.74 to 440.60 nm and CPHO at 178.95 to 434.08 nm. The highest stabilization energy of NPHO is LP (1) N_{12} donor and LP*(1) H_{10} acceptor with a value of 417.54 kcal/mol compared to πC_{17} - O_{18} donor and $\pi^* C_{19}$ - C_{28} acceptor with a value of 108.33 kcal/mol for CPHO. The molecular binding affinity of CPHO and NPHO had a high mean binding affinity of -5.83 and -6.05 kcal/mol, compared to the standard antiviral drugs with -5.00 kcal/mol. Therefore, the compounds show excellent reactivity based on the electronic structure, spectroscopic characterization and represent a potential antiviral agent treatment for HBV and HCV.

1 INTRODUCTION

Hepatitis B and C infections are one of the biggest worldwide health challenges, and both cause chronic and acute infection in humans, despite the numerous medicines proposed by scientists.[1-3] The liver remains the target that can be damaged by hepatitis B and C. According to the World Health Organization (WHO, 2019), hepatitis affects around 325 million people globally, with viral hepatitis B and C causing approximately 1.4 million fatalities each year.[4, 5] Hepatitis is the second leading cause of death in the world. People are 9 times more likely to get hepatitis than they are to

contract HIV after tuberculosis.[6] Cirrhosis, hepatic decompensation, and hepatocellular cancer are among the clinical disorders induced by hepatitis B and C infection.[7-9] Hepatitis B virus DNA is double-stranded and belongs to the *Hepadna-viridae* family.[10, 11] However, Interferon (IFN-a, including non-pegylated and pegylated) and nucleoside analogues are now FDA-approved HBV inhibitors for antiretroviral therapy (lamivudine, adefovir, tenofovir, telbivudine, and entecavir).[12] Both therapy methods have been shown in numerous clinical trials to lower HBV DNA concentration in liver cells, block HBV replication, and slow the progression of liver disease. However, adverse effects and drug resistance are common problems with anti-HBV medicines, limiting their use as antiviral treatments.[13, 14] As a result, it appears that numerous pathways will need to be addressed to have a clinically significant impact on the persistent viral reservoir. On the other hand, hepatitis C is an infectious disease that damages the liver and is usually caused by the hepatitis C virus. Hepatitis C is an RNA virus with a tiny size, single-stranded RNA, that attacks liver cells.[15] The virus belongs to the Flaviviridae family, which causes not just hepatitis but also liver cancer, cirrhosis, and lymphoma in humans.[16] Typically, no symptoms occur during the early stages of illness. However, late in the course of a persistent infection, significant symptoms occur, causing 60-70 per cent of the liver tissues to be damaged.[15-17]

Quantum chemistry approaches have been proven to be effective in establishing the molecular structure as well as the electronic structure and reactivity of several physiologically relevant compounds.[18] Although there are various quantum chemical approaches accessible presently, methods based on density functional theory (DFT) have gained a lot of interest due to their better balance between processing cost and accuracy.[19] Generally, DFT methods give the electronic energy and related parameters as a function of electron density, which is a function of position coordinates. The exchange and correlation elements of the energy functional are approximated differently by these methods. In the absence of experimental data, currently, available DFT algorithms are completely capable of reproducing structural characteristics (bond lengths, bond angles, etc.) and spectral parameters (FT-IR, NMR, UV-Vis, etc.) and providing credible predictions of the same.[18, 19]

This research work aims to synthesize two compounds (CPHO and NPHO), characterize, and determine their reactivity using DFT which involves geometry optimization of synthesized compounds, UV-VIS analysis to determine the excitation of atom groups, FT-IR to determine their vibrational modes and frequencies, non-linear optics to determine its optoelectronic properties, Fukui function to establish the reactive sites, TDOS to determine the electron density distribution, and perform molecular docking to determine its suitability for drug formulation for the treatment of Hepatitis B and C.

2 MATERIALS AND METHODS

2.1 Synthesis of compounds of CPHO and NPHO

A cold solution of the diazonium salt (10 mmol) (prepared by adding a cold solution of sodium nitrite (0.7 g) in water (5 mL) to a solution of the aniline (10 mmol) in conc. hydrochloric acid (5 mL) was added to a cold solution of enaminone (10 mmol) in ethanol (10 mL) containing sodium sulphate (2 g) according to Ref. [20]. The mixture was stirred at room temperature for 1 h, and the solid precipitate that formed was collected by filtration and crystallized from proper solvents to give yellow crystals according to scheme 1a-1. The detail characterizations of the synthesized structures are shown in table 1.

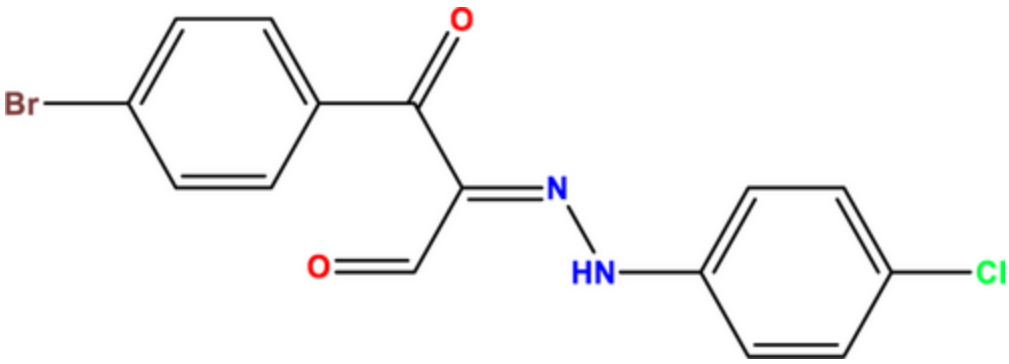

Scheme 1a

Open in figure viewerPowerPoint

(E)-3-(4-bromophenyl)-2-(2-(4-chlorophenyl)hydrazineylidene)-3-oxopropanal (CPHO)

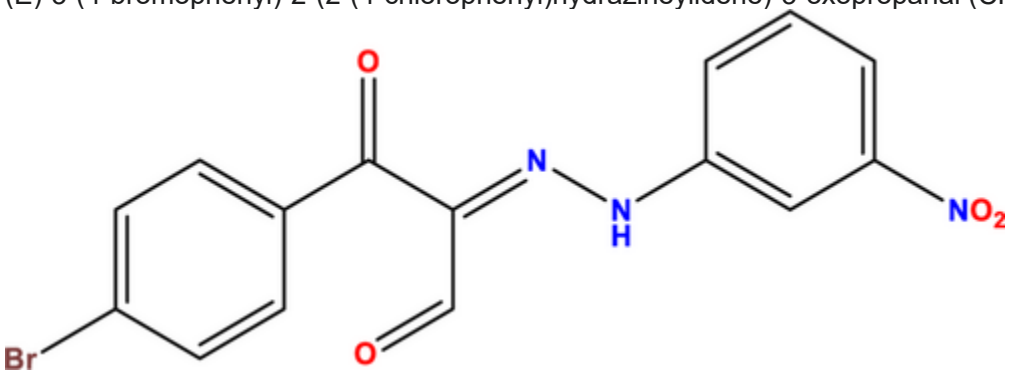

Scheme 1b

Open in figure viewerPowerPoint

(E)-3-(4-bromophenyl)-2-(2-(3-nitrophenyl)hydrazineylidene)-3-oxopropanal (NPHO)

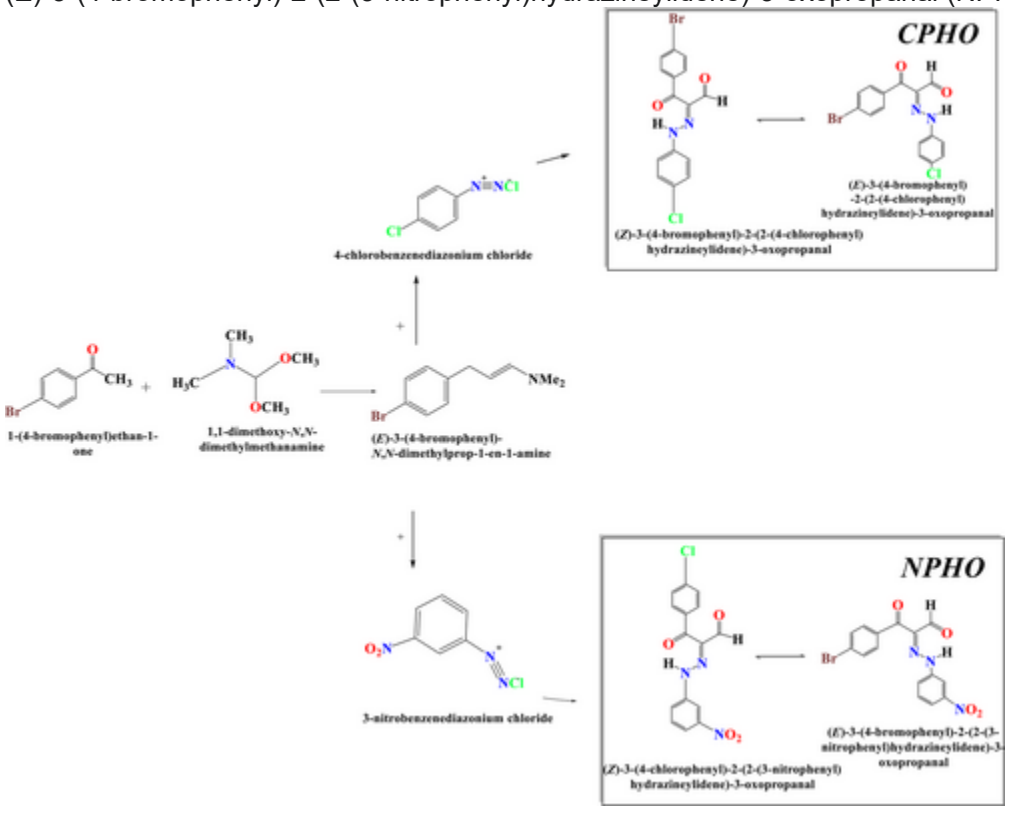

Scheme 1
Open in figure viewerPowerPoint
Synthetic pathway of CPHO and NPHO

Table 1. Experimental yield and FT-IR frequencies of CPHO and NPHO

Compounds	Yields (%)	Melting point (°C)	Anal. Calc.	FT-IR (cm^{-1})
CPHO	**85**	**162**	(365.61), C, 49.28; H, 2.76; N, 7.66. Found: C, 50.66, H, 2.76, N, 7.92; MS m/z (M)+ = 365.06	3069 (NH), 1645 (CO)
NPHO	**82**	**210**	(376.16), C, 47.89; H, 2.68; N, 11.17. Found: C, 47.75, H, 2.50, N, 10.91; MS m/z (M)+ = 376.10	3092 (NH), 1641 (CO)

2.2 Computational **methods**

The electronic property of the synthesized compounds was investigated using Density Functional Theory (DFT), which is an electronic structural theory method for investigating the electronic properties of atoms and molecules.[21] The compound's structure was optimized at the B3LYP functional and 6-311++G(d,p) basis set and visualized using the Gaussian16 and GaussView 16 softwares respectively.[22, 23] To elucidate the thermodynamic properties of the molecules, frequency calculations were performed at the same level of theory using the CPCM solvation model for the water, ethanol and DMSO solvent media. TD-SCF/ B3LYP/6-311++G(d,p) theoretical methods were used to calculate theoretical UV-VIS excitation energies for the first singlet states. Multiwfn program was used to determine the reactive sites, polarizabilities, and other related molecular properties of the studied molecule.[24]

3 RESULTS AND DISCUSSION

3.1 Frontier molecular orbital (FMO)

The frontier molecular orbital (FMO) describes the boundaries of electron occupancy in a molecule, which is symbolized by the connection of the HOMO and LUMO.[25] The HOMO is a nucleophile, whereas the LUMO is an electrophile. As shown in figure 1, 2, the energy gap characterizes the ability of electron injection from the HOMO to the LUMO and hence the extent of reactivity of the molecule, with values of 2.545 and 3.520 eV for NPHO and CPHO, respectively.

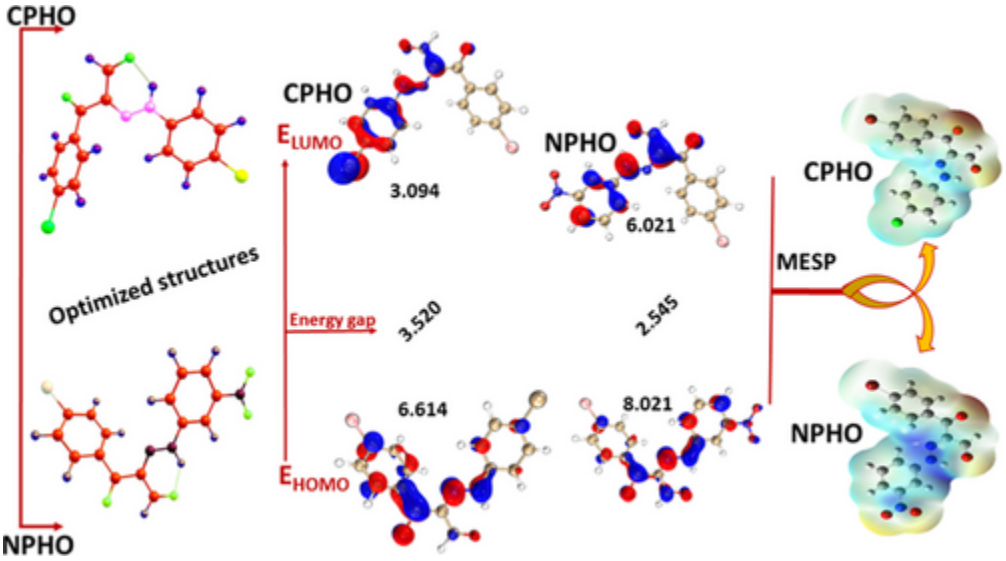

Figure 1

Open in figure viewerPowerPoint

The 3D structure HOMO-LUMO diagram, and electrostatic potential of CPHO and NPHO

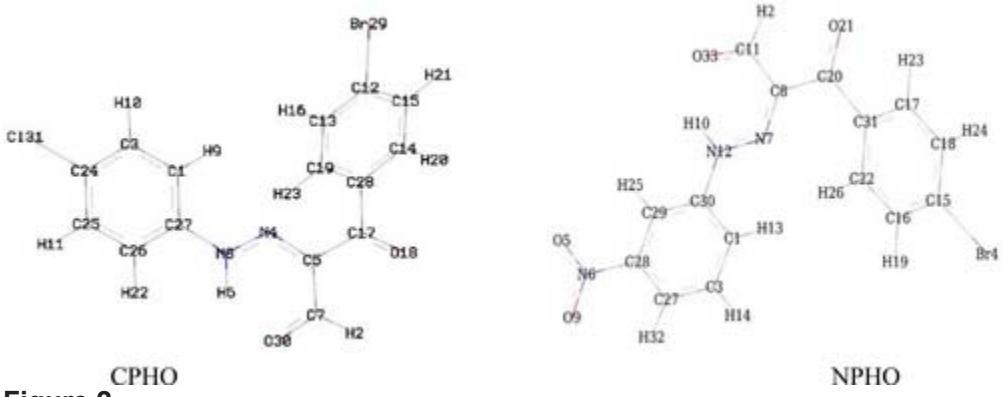

Figure 2

Open in figure viewerPowerPoint

Wireframe structure of CPHO and NPHO showing the atom labels and numbers

The Koopmans approximation defines the ionisation energy required to remove the most loosely bound electron to be HOMO, as well as the electron affinity, which is the energy lost when placing an electron to be the LUMO, and was used to construct the quantum descriptor (QD) displayed in table 2. The electronegativity (χ) demonstrates the simplicity with which electrons can be polarized. Lower

Table 2. Quantum descriptors of *CPHO* and *NPHO* calculated at the DFT/6-311++G(d, p) method

Quantum descriptors	CPHO	NPHO
E_{LUMO} (eV)	-3.094	-6.021
E_{HOMO} (eV)	-6.615	-8.567

Quantum descriptors	CPHO	NPHO
I (eV)	6.614	8.021
A(eV)	3.094	6.021
Energy gap (eV)	3.520	2.545
χ (eV)	-4.854	-7.293
n (eV)	3.521	1.272
ω (eV)	3.346	20.90
μ (eV)	4.854	7.293
S (eV)	0.142	0.393

electronegativity levels indicate a high effective nuclear charge and are higher in NPHO and CPHO, with values of -7.293 eV and -4.854 eV, respectively.Chemical species are classified as 'hard' (n) or 'soft' (S) depending on their charges and polarizability. Small, high-charge states and species with weak polarizability are classed as "hard." Soft species are big, have low charge states, and are highly polarizable.[26] The calculated hardness (*n*) and softness (S) values of 1.272 and 0.393 eV for NPHO, and of 3.521 and 0.142 eV for CPHO which also confirms NPHO to be more reactive compared to CPHO**.** The electrophilicity index which is the ability of a molecule to act as an electron sink is much higher in NPHO with a value of 20.90 eV compared to CPHO with a value of 3.346 eV and agrees with the small energy gap/electron affinity values. The chemical potential (μ) describes the energy required by a molecule to initiate a chemical or a thermodynamic reaction which is due to a disequilibrium in the reactant or product species and this is energy higher in NHPO with a value of 7.293 eV compared to CPHO with a value of 4.854 eV. The electronegativity (χ), electrophilicity index (ω), softness (S), and hardness (n) are termed DFT quantum chemical descriptors and are calculated using the equations below and the HOMO and LUMO are approximated, based on Koopmans, to be the ionization energy (I) and the electron affinity (A), respectively.[27]

$$I = -E_{HOMO} \quad (1)$$

$$A = -E_{LUMO} \quad (2)$$

$$\chi = -\mu = \frac{I+A}{2} \quad (3)$$

$$n = \frac{I-A}{2} \quad (4)$$

$$S = \frac{1}{2n} \quad (5)$$

$$\omega = \frac{\mu 2}{2n} \quad (6)$$

where μ denotes the chemical potential of the system. The DFT quantum chemical distributors explain the reactivity of a molecule. Table 2 shows the quantum chemical descriptors of CPHO and NPHO.

3.2 FT-IR vibrational analysis

By generating an infrared absorption spectrum, Fourier Transform Infrared Spectroscopy (FT-IR) findings shows information about the chemical bonds, functional groups, and vibration modes of atoms and molecules.[27, 28] The detail vibrational modes, FT-IR frequencies, and functional group assignment of CPHO and NPHO structure in four solvent phases are shown in table 3.

Table 3. FT-IR frequencies of CPHO and NPHO structure in four solvent phases

	CPHO (gas)	**CPHO (water)**	**CPHO (ethanol)**	**CPHO (DMSO)**	**NPHO (gas)**	**NPHO (water)**	**NPHO (ethanol)**
Mode	FT-IR Frequency (cm^{-1})	FT-IR Frequency (cm^{-1})	FT-IR Frequency(cm^{-1})	FT-IR Frequency (cm^{-1})	FT-IR Frequency (cm^{-1})	FT-IR Frequency (cm^{-1})	FT-IR Frequency (cm^{-1})
H-C=C-H	vs3236.04, vs3231.84, vs3225.02, vs3224.71, va3218.03, va3214.44, va3211.20, va3192.55, vs3053.73, vs859.0, vs864.84 δ1642.22, δ1134.23, δ1633.48, τ995.66, τ982.05, ω840.88, ω796.49, δ1439.34, ρ1325.15,	vs3240.65, vs3234.31, vs3229.42, vs3226.86, vs3226.86, va3222.51, va3219.33, va3212.69, va3205.11, vs3053.24, ρ1521.81, ρ1515.52,	vs 3240.47, vs 3234.17, vs3229.25, vs 3226.82, va3222.36, va3219.15, va3212.71, va3204.68, vs3053.46, ρ1521.94, ρ1515.60, δ1452.25,	vs3240.27, vs3234.27, vs3229.37, vs3226.84, va3222.46, va3219.27, va3212.69, va3204.98, vs3053.31, ρ1521.85, ρ1515.54, δ1452.07,	vs3054.96, va3208.40, va3211.54, va3214.45, vs3225.00, vs3231.01, vs3237.54, vs3249.38, ω841.31, τ981.84, δ1134.23, δ1184.51, δ1205.04, β1408.79, ρ1517.33, ρ1329.49, ρ1325.57	vs3254.77, vs3242.93, vs3237.52, vs3234.35, vs3227.17, va3220.17, va3219.23, va3213.53, vs3055.01, ρ1516.50, ρ1514.33, δ1423.61,	vs3254.3 vs3242.7 vs3237.1 vs3234.1 vs3227.1 va3219.9 va3218.8 va3213.3 vs3055.1 ρ1516.6 ρ1514.5 ρ1482.6

	CPHO (gas)	CPHO (water)	CPHO (ethanol)	CPHO (DMSO)	NPHO (gas)	NPHO (water)	NPHO (ethanol)
	δ1409.31, δ1205.04	δ1451.99, δ1430.05, δ1421.22, vs1414.45, ρ1326.01, ρ1322.63, ρ1314.80, δ1202.48, δ1188.76, δ1133.57, δ1131.54,	δ1430.45, δ1421.46, vs1414.32, β1414.32, ρ1325.99, ρ1322.60, ρ1314.79, δ1202.57, δ1188.79, δ1170.14, δ1133.61, δ1131.53, ρ1017.46, τ992.48, τ986.56, ω858.44, ω848.45, ω841.71, ω840.56, ω794.12	δ1430.18, β1414.41, ρ1326.00, ρ1322.62, ρ1314.80, ρ1233.80 δ1202.51, δ1188.77, δ1133.58, δ1131.54, τ992.44, τ986.66, ω858.36, ω841.64 ω840.57, ω839.12, ω734.69, ω710.52, ω534.29		β1413.92, ρ1337.01, ρ1328.16, ρ1324.01, δ1203.68, δ1183.03, ρ1135.06, τ994.30, τ987.35, ω857.79, ω841.39	δ1423.7 δ1203.7 δ1335.0
N-H	v3330.53, β1582.80	v3331.18, β1574.49	v3330.11, β1574.82	v3330.85, β 1574.60,	v846.32, β1582.36, vs3309.81,	v3336.37, β1570.66	v3335.4 β1571.1

	CPHO (gas)	CPHO (water)	CPHO (ethanol)	CPHO (DMSO)	NPHO (gas)	NPHO (water)	NPHO (ethanol)
							β822.26
C=O	v1700.31, v1687.41	v1679.15, v1655.36, v1430.05	v1679.89, v1656.62,	v1679.38, v1655.76, v1430.18	v1705.60, v169.14,	v1685.55, v1660.65,	v1686.3 v1662.0
C=C	vs908.61, va1021.06, va1642.22	va1636.06, va1630.33, va1626.47, va1604.42, va1349.24, va1341.62	va1636.26, va1630.40, va1626.78, va1604.56, va1349.18, va1341.71	va1636.13, va1630.35, va1626.57, va1604.47, va1521.85, va1349.22, va1341.65, vs1233.80, τ 420.67	va1667.22, va1633.34, va1517.33, va1377.42, va1345.46,	va1659.09, va1632.88, va1627.88, va1627.01, va1604.63, va1378.74, va1343.24	va1659. va1633. va1627. va1604. va1378. vs1009. vs1009.
C-N	vs1236.12, vs1460.33	vs1430.05, vs1421.22, vs1233.78	vs1452.25, vs1430.45, vs1421.46, vs1233.86	vs 1430.18 vs 1421.30	vs1519.98 vs1383.52 vs1490.93, vs1445.64,	vs1514.33 vs1516.50 vs1560.40	vs1562. vs1516.
N-N	vs1344.12, vs1340.21	vs1353.27, vs1349.24	vs1352.86, vs1349.18	vs 1353.14	vs1325.57, vs1329.49, vs1322.44	vs1337.38,	vs1336.

	CPHO (gas)	CPHO (water)	CPHO (ethanol)	CPHO (DMSO)	NPHO (gas)	NPHO (water)	NPHO (ethanol)
C-C	vs1166.80, vs971.83	vs1170.25	vs1170.14, vs968.93	vs1170.22 vs968.86	vs1166.39	vs1170.25	vs1170. vs965.1
C-Cl	vs1106.13	vs1097.45	vs1097.74	vs1097.54	-	-	-
C-Br	vs1093.33	vs1088.09	vs1088.27	vs1088.14 vs1021.48	1093.45	vs1088.44	vs1088.
NO_2	-	-	-	-	va1604.51, vs1383.52	va1560.40, vs1368.76, δ830.59	va1562. vs1369. δ830.68

3.2.1 C-H vibrations

The maximum aromatic C-H stretching vibrations was observed for NPHO and CPHO in gas, water, ethanol and DMSO with symmetric vibrations at frequencies NPHO (3249.38, 3254.77, 3254.59, 3254.71 cm^{-1}) and CPHO (3236.04, 3240.66, 3240.47, 3240.27 cm^{-1}) respectively, asymmetric stretching vibrations at NPHO (3214.45, 3220.17, 3219.93, 3220.99 cm^{-1}), CPHO (3218.03, 3222.51, 3222.36, 3222.46 cm^{-1}), respectively. Some scissoring modes were also observed between 1600 to 1000 cm^{-1}, twisting modes between 1000 to 900 cm^{-1}, rocking modes between 1500 to 1000 cm^{-1}, and wagging modes between 900 to 700 cm^{-1}. The frequency of C-H aromatic stretching is expected to be between 3100 and 3000 cm^{-1}, resulting in a mild intensity. The solvent effect causes the frequencies measured in water, ethanol, and DMSO to be somewhat higher than those observed in the gas phase. The inductive effects of the electron-withdrawing groups of chlorine and bromine in CPHO cause the frequencies of CPHO to be somewhat higher than those of NPHO. The NO_2 group on NPHO enables the molecule to have a stronger mesomeric influence. The reported stretching frequencies are higher than the estimated frequencies, suggesting that the molecule has redshifted.[28]

vs – symmetric stretching; va – asymmetric stretching; δ – scissoring; ρ – rocking;

ω – wagging; τ – twisting; β – single atom bending.

3.2.2 N-H vibrations

The N-H maximum stretching vibrations was observed for NPHO and CPHO in gas, water, ethanol and DMSO at frequencies; NPHO (3309.81, 3336.37, 3335.44, 3336.08 cm^{-1}), CPHO (3330.53, 3331.18, 3330.11, 3330.85 cm^{-1}) and maximum bending vibrations at NPHO (1582.36, 1570.66, 1571.14, 1570.81 cm^{-1}), CPHO (1582.80, 1574.49, 1574.82, 1574.60 cm^{-1}). The estimated frequency

of secondary amine is between 3350 to 3310 cm^{-1}. The observed stretching frequencies fall within the estimated frequency range.[28]

3.2.3 C=O/C=C vibrations

The C=O maximum stretching vibrations was observed for NPHO and CPHO in gas, water, ethanol and DMSO at frequencies; NPHO (1705.60, 1685.55, 1686.31, 1685.79 cm^{-1}), CPHO (1700.31, 1679.15, 1679.89, 1679.38 cm^{-1}). The estimated frequency is between 1740 to 1720 cm^{-1}.[28] The conjugation from the benzene ring attached to the C=O functional group lowers the frequencies by about 30 cm^{-1}. The C=C symmetric and asymmetric stretching vibrations are observed between the C=C of the benzene ring. The asymmetric stretching of C=C is observed.

3.2.4 C-N/N-N vibrations

The maximum aromatic C-N stretching vibrations were observed for NPHO and CPHO in gas, water, ethanol and DMSO at frequencies; NPHO (1519.98, 1560.40, 1562.06, 1514.40 cm^{-1}) and CPHO (1460.33, 1430.05, 1452.25, 1430.18 cm^{-1}) respectively. The estimated frequency for C-N vibration is between 1342-1266 cm^{-1} producing strong intensity. A red-shift is also observed when comparing the estimated frequency to the observed frequencies. The N-N maximum stretching vibration is observed for NPHO and CPHO in gas, water, ethanol and DMSO at frequencies; NPHO (1325.57, 1337.38, 1336.91, 1337.23 cm^{-1}) and CPHO (1344.12, 1353.27, 1352.86, 1353.14 cm^{-1}) respectively. The estimated N-N stretching is observed between 1180-1080 cm^{-1}.[28] The observed frequency is higher than the estimated frequencies suggesting a red-shift.

3.2.5 C-C/C-Cl/C-Br/NO_2 vibrations

The C-C maximum stretching between the carbonyl carbon and the aromatic carbon was observed for NPHO and CPHO in gas, water, ethanol and DMSO at frequencies; NPHO (1166.39, 1170.25, 1170.12, 1170.21 cm^{-1}), and CPHO (1166.80, 1170.25, 1170.14, 1170.22 cm^{-1}). These frequencies are usually observed at the fingerprint region of the IR spectrum. The frequencies of both compounds in solvent phases remained the same and differs from the frequencies in the gaseous phase. The C-Cl stretching was observed only for CPHO in gas, water, ethanol and DMSO at frequencies; CPHO (1106.13, 1097.45, 1097.74, 1097.54 cm^{-1}). A slight decrease in frequency was observed when the compound was solvated but the frequencies in the solvent phases remained relatively the same. The C-Br maximum stretching mode was also observed for NPHO and CPHO in gas, water, ethanol and DMSO at frequencies; NPHO (1093.45, 1088.44, 1088.60, 1088.49 cm^{-1}) and CPHO (1093.33, 1088.09, 1088.27, 1088.14 cm^{-1}). There is also a decrease in the frequency of C-Br stretching when solvated. The NO_2 symmetric and asymmetric stretching was observed only for NPHO in gas, water, ethanol and DMSO. The asymmetric stretching was observed at frequency; 1604.51, 1560.40, 1562.06, 1560.92 cm^{-1} and symmetric stretching at 1383.52, 1368.76, 1369.56, 1369.01 cm^{-1} in gas, water, ethanol and DMSO respectively.

3.3 UV-Vis analysis

UV-Vis spectroscopy data reveals the wavelength and intensity of ultraviolet and visible photons of light absorbed by a compound.[29, 30] The ease with which electrons can be excited from the ground state is related to the wavelength of absorption and indirectly related to the energy of excitation. These measurements aid in determining the optical and electronic properties (transmittance, reflectance, and absorbance) of molecules and can be used to investigate semiconductor materials, coatings, and a variety of other manufacturing materials. The estimated result including the vertical excitation energy, oscillation strength (f), and wavelength (λmax) is performed and compared to the

measured experimental wavelength reported in table 4. Generally, the highest absorption peak max in the UV-Vis spectrum correlates to vertical excitation, according to the Frank–Condon concept. Absorption wavelengths over 400 nm form coloured compounds due to high conjugation and are within the visible spectrum range, whereas wavelengths below 400 nm produce colourless compounds and are inside the UV zone. The NPHO absorption spectrum revealed three high excitation energy bands at 369.74 nm, 377.30 nm, and 440.60 nm, while the CPHO absorption band revealed three high wavelength absorption bands at 357.25 nm, 178.95 nm, and 434.08 nm. These bands in the high-energy region are caused by the intraligand n–π* electronic transition in the chromophore. The π–π* electronic transition caused by the implicated molecular orbitals is essential for the weak and broad absorption bands detected at 440.60 nm for NPHO and 434.08 nm for CPHO. For NPHO, the excitation state $S_o \rightarrow S_2$ (94→95) accounts the highest major contribution of 63.34 % while for CPHO, $S_o \rightarrow S_2$ (91→92) excitation has the highest major contribution of 93.98 %. The oscillatory strength expresses is the probability of a molecule emitting or absorbing radiation on the transition between energy levels. The higher the oscillatory strength, the brighter the transition. NPHO has its highest oscillatory strength of 0.1069 in the $S_o \rightarrow S_2$ (94→95) transition state and CPHO has its highest oscillatory strength of 0.5133 in the $S_o \rightarrow S_2$ (91→92) transition state. The oscillatory strength is also directly proportional to the contributions of the energy states.

Table 4. UV-Vis excitation states, energy and oscillatory strength of CPHO and NPHO

Excitation state	Wavelength (nm)	Energy (eV)	Oscillatory strength (f)	Major contribution (%)	Assignment
CPHO					
$S_o \rightarrow S_1$ (90→92)	434.08	2.8562	0.0034	47.12	n–π*
$S_o \rightarrow S_2$ (91→92)	378.95	3.2718	0.5133	93.58	π–π*
$S_o \rightarrow S_3$ (90→92)	357.25	3.4705	0.0273	44.32	π–π*
NPHO					
$S_o \rightarrow S_1$ (92→95)	440.60	2.8140	0.0024	46.79	n–π*
$S_o \rightarrow S_2$ (94→95)	377.30	3.2861	0.1069	63.34	π–π*
$S_o \rightarrow S_3$ (93→95)	369.74	3.3533	0.0220	50.68	π–π*

3.4 Nonlinear optics (NLO) analysis

Nonlinear optics (NLO) explores the inelastic and elastic optical redirection that occurs when high-intensity lasers interact with the material. Polarization is generated by dislodged charged particles. When a dipole moment is formed in a substance, this becomes polarizable. Static polarizabilities, on the other hand, are used to investigate intramolecular and intermolecular interactions in a

molecule. [31] It is the electron density's initial response to applied electric field, and it is correctly predicts the handling of the excited state by density functionals. The fundamental goal of this objective is to undertake a theoretical analysis of the structural, electrical, and optical properties of CPHO and NPHO. NLO materials can be created from molecules with high hyperpolarizability values, and they have numerous applications in communication science and technology. Nonlinear optical materials have gained popularity in recent years due to their potential utility in domains such as laser technology, optical communication, optical data storage, and optical signal processing. It also aids in a wide range of optoelectronics and photonics purposes. Organic chromophores have strong and fast nonlinearities, making them a suitable inorganic material substitute. This is due to their proclivity for causing electron delocalization.[32] Asymmetric polarisation induced by electron donor and electron acceptor groups on both side of the molecule at relevant locations in the molecular systems is used to develop effective organic materials for non-linear optical effects.[33] The Gaussian 16 software was used to perform the computations. Polarizabilities were estimated instantly during NPHO and CPHO geometry optimization, and NLO descriptors were derived using log file coordinate data. The frequency-dependent electronic hyper-polarizability and static polarizability βxyz and αxyz were calculated using the Coupled-Perturbed Hartree-Fock technique. The basis set can be used to compute molecule polarizabilities.[30] The NLO descriptors where obtained from the output Gaussian log file. The dipole moments (μ), polarizability anisotropies (α), isotropically averaged polarizabilities (Δα), and isotropically first-order hyperpolarizabilities (βtotal), which were calculated using equations below, were among the parameters obtained.

$$\mu = \sqrt{\mu 2x + \mu 2y + \mu 2z} \quad (7)$$

$$\langle \alpha \rangle = \frac{1}{3}(\alpha xx + \alpha yy + \alpha zz) \quad (8)$$

$$\Delta \alpha_{total} = \{\frac{1}{2}[(\alpha xx - \alpha yy)^2 + (\alpha xx - \alpha zz)^2 + (\alpha yy - \alpha zz)^2 + 6(\alpha^2 xy + \alpha^2 xz + \alpha^2 yz)]\}^{1/2} \quad (9)$$

$$\beta_{total} = \sqrt{\beta 2x + \beta 2y + \beta 2z} \quad (10)$$

where

$$\beta_x = \beta_{xxx} + \beta_{xyy} + \beta_{xzz} \quad (11)$$

$$\beta_y = \beta_{yyy} + \beta_{xxy} + \beta_{yzz} \quad (12)$$

$$\beta_z = \beta_{zzz} + \beta_{xzz} + \beta_{yyz} \quad (13)$$

Table 5 showed NPHO exhibited high dipole moments (μ), polarizability anisotropies ⟨α⟩, isotropically averaged polarizabilities ($\Delta\alpha_{total}$), and isotropically first-order hyperpolarizabilities (β_{total}) with values 3.94 D, -67.38 a.u., 446.65 a.u., and 490.49 a.u., respectively compared to CPHO with values 2.21 D, -146.83 a.u., 25.91 a.u., and 250.77 a.u. This is due to the high level of conjugation and electron delocalization within the molecule which agrees with the NBO stabilization energy values. Therefore, suggests that NPHO has higher optical stability compared to CPHO.

Table 5. NLO descriptors for compounds CPHO and NPHO

	CPHO	**NPHO**
Dipole moment (D)		
X	**1.52**	**-3.17**

	CPHO	NPHO
Y	-1.50	-2.31
Z	0.57	0.31
μ	2.21	3.94
Static Polarizability (a.u.)		
Axx	-141.23	-189.45
αXY	5.70	4.04
αYY	-159.03	-154.92
αXZ	3.44	-1.74
αYZ	0.86	1.45
αZZ	140.23	142.22
α_{Total}	-146.83	-67.38
Δα	25.91	446.65
Static hyperpolarizability (a.u.)		
βXXX	-86.82	-472.96
βXXY	5.30	32.13
βXYY	-57.64	-44.06
βYYY	-139.78	-130.80
βXXZ	-6.04	-41.67

	CPHO	NPHO
βXYZ	-1.65	3.88
βYYZ	6.93	3.49
βXZZ	55.09	40.95
βYZZ	-17.29	-15.99
βZZZ	4.36	10.11
βX	-199.56	-476.07
βY	-159.77	-114.67
βZ	5.44	-28.06
β_{Total}	250.77	490.49

3.5 Fukui function

Fukui function, which is an extension of Fukui's frontier MO reactivity index, is a major aspect of conceptual DFT, which finds expressions with chemical properties that science could utilise on a strictly evidential basis in most circumstances.[34, 35] It is the number of electrons derivative of the electron density. Since electron density differs with the number of electrons, a left-hand and right-hand side derivative is initiated, with f -A used to investigate reactivity when electrons are added to the system (attack of a nucleophile) and f +A used to investigate reactivity when electrons are eliminated (attack of a nucleophile) (attack of a electrophile). The bigger the value of the Fukui function, the higher the overall reactivity of the relevant site. The f+A function computes the change in electron density caused by the addition of one electron. The higher the f+ value at the nucleophilic attack site r, the more electrons it can absorb (on an atom in a molecule). As a result, an atom with a higher f+A value in a molecule is more vulnerable to nucleophilic assault. The value of the local f+A function should be used to determine electrophilicity at the reaction site in this case. A molecule's atom with a high fA value is also vulnerable to electrophilic attack, hence it should now be used to indicate nucleophilicity. The regioselectivity is calculated using the values of the f+A and fA functions. Electrophilicity and nucleophilicity are quantitative measurements of an atom's ability to accept or contribute electrons in a molecule. Hirshfeld's charge can correctly quantify electrophilicity and nucleophilicity as well as regioselectivity.

The Hirshfeld charges of all the atoms in NPHO and CPHO were estimated in their N, N+1, and N+2 electron states. The condensed Fukui functions and dual descriptors were also calculated using the formula. In the table above, the Hirshfeld charges of chosen atoms in NPHO and CPHO are

displayed. The atoms O_{22}, C_7 and O_{23} in NPHO have the smallest two values for f^-, making them the most unfavourable site for an electrophilic attack. Positive values for the dual descriptor are found at C_7, C_9, C_{11}, N_{21}, O_{23}, with the highest positive value at C_7, indicating that it is the most unfavourable site for electrophilic attack. For CPHO, the smallest value for f^- occurs at C_4, suggesting that it is the most unfavourable site for an electrophilic attack. For dual descriptor, the highest positive value is at C_4 which also suggests that it is an unfavourable site for electrophilic attack. Tables 6a and 6b show the condensed the selected Fukui functions of NPHO and CPHO.

Table 6a. Condense Fukui function and electrophilicity of CPHO

Atom	q^A (N)	q^A (N+1)	q^A (N-1)	f^-_A	f^+_A	Δf_A
4(C)	-0.0390	-0.1473	-0.0265	0.0125	0.1083	0.0958
7(C)	0.1227	0.0529	0.1549	0.0321	0.0698	0.0377
18(C)	-0.2511	-0.3260	-0.2078	0.0433	0.0750	0.0317
1(C)	-0.0415	-0.0693	-0.0054	0.0361	0.0278	-0.0082
2(C)	0.0508	0.0138	0.0745	0.0238	0.0369	0.0132
3(C)	-0.0357	-0.0598	-0.0032	0.0326	0.0241	-0.0085
7(C)	0.1227	0.0529	0.1549	0.0321	0.0698	0.0377

Table 6b. Condense Fukui function and electrophilicity of NPHO

Atom	q^A (N)	q^A (N+1)	q^A (N-1)	f^-_A	f^+_A	Δf_A
5(C)	-0.1985	-0.2622	-0.1704	0.0281	0.0637	0.0355
7(C)	-0.0390	-0.1192	-0.0257	0.0133	0.0803	0.0670
9(C)	-0.1973	-0.2631	-0.1635	0.0338	0.0658	0.0320
11(C)	0.1270	0.0682	0.1567	0.0298	0.0588	0.0290
21(N)	-0.2470	-0.3087	-0.2045	0.0424	0.0617	0.0192
22(O)	-0.0290	-0.0275	-0.0181	0.0109	-0.0015	-0.0124

Atom	q^{A} (N)	q^{A} (N+1)	q^{A} (N-1)	f^{-}_{A}	f^{+}_{A}	Δf_{A}
23(O)	0.0541	0.0446	0.0693	0.0152	0.0095	-0.0058
1(C)	-0.0321	-0.0808	-0.0028	0.0292	0.0488	0.0195
2(C)	0.0527	0.0206	0.0757	0.0231	0.0320	0.0090
3(C)	-0.0221	-0.0522	0.0075	0.0297	0.0301	0.0004

3.6 Natural bond orbital (NBO) analysis

The Natural Bond Orbital (NBO) characterizes the intermolecular and intramolecular interplay within and between a molecule or compound as a result of micro disturbances or perturbation, as well as electron density delocalization patterns from the bonding orbital to the antibonding orbital. The NBO information was produced immediately during the structure geometries optimization process. [36] The amplitude of each donor NBO I and acceptor NBO (j) stabilization energy, as well as E2 associated with electron delocalization between the donor and

acceptor, was anticipated using the second-order energy model,

$$E^{(2)} = n\sigma \frac{(F_{i,j})^2}{\varepsilon_j - \varepsilon_i} \quad (14)$$

where F(ij) denotes the off-diagonal Fock-matrix elements, E(j)E(i) the orbital energy differential between the donor and acceptor NBOs, and n the donor population orbital.[37] NBO analysis can be used to investigate intramolecular and intermolecular bonding and interactions between bonds, as well as charge transfer and conjugative interactions in molecular systems. Tables 7a-7b present numerous electron donor orbitals, acceptor orbitals, and the interaction stabilisation energy derived using second order micro-disturbance theory. The stabilisation energy explains the donor-acceptor orbital interaction (E^2). The bigger the E^2 value, the more intense the interaction between electron donors and the more extensive the system conjugation. When electron density delocalizes between occupied Lewis type (bond or lone pair) NBO orbitals and technically unoccupied non-Lewis NBO orbitals (antibonding or Rydberg), a stabling donor-acceptor interaction ensues. The highest stabilization energy of NPHO is observed between LP (1) N_{12} donor and LP*(1) H_{10} acceptor with a value of 417.54 kcal/mol compared to that of CPHO observed between πC_{17}-O_{18} donor and $\pi^* C_{19}$-C_{28} acceptor with a value of 108.33. the high stabilization energies of NPHO indicates an intensive intermolecular interaction, electron delocalization and a high level of conjugation within the molecule compared to CPHO. This is also due to the small energy gap of 2.545 eV compared to CPHO of 3.520 eV which allows ease of excitation of electrons from the HOMO to the LUMO.

Table 7a. NBO second-order perturbation donor and acceptor orbitals for CPHO

Donor (i)	Acceptor (j)	$E^{(2)}$/(kcal/mol)	$E(i)-E(j)$ (a.u.)	$F(i,j)$ (a.u.)
πC_{17} - O_{18}	$\pi^* C_{19}$ - C_{28}	108.33	0.01	0.063

Donor (i)	Acceptor (j)	$E^{(2)}$/(kcal/mol)	E(i)−$E(j)$ (a.u.)	$F(i,j)$ (a.u.)
πC_{12} - C_{13}	$\pi^* C_{19}$ - C_{28}	167.48	0.02	0.084
πC_{12} - C_{13}	$\pi^* C_{14}$ - C_{15}	126.75	0.02	0.078
πN_4 - C_5	$\pi^* C_7$ - O_{30}	118.13	0.02	0.079
πN_8 - C_{27}	$\pi^* C_{25}$ - C_{26}	81.57	0.08	0.093
πN_8 - C_{27}	$\pi^* N_4$ - C_5	58.12	0.04	0.054
πN_8 - C_{27}	$\pi^* C_1$ - C_3	79.38	0.08	0.095
LP (1) C_{24}	$\pi^* C_{25}$ - C_{26}	58.53	0.16	0.104
LP (1) C_{24}	$\pi^* C_{12}$ - C_{13}	55.77	0.17	0.104
πC_{25} - C_{26}	LP (1) C_{24}	52.57	0.12	0.089
πC_1 - C_3	LP (1) C_{24}	53.69	0.11	0.089
πC_1 - C_3	$\pi^* N_8$ - C_{27}	33.47	0.20	0.085

Table 7b. NBO second-order perturbation donor and acceptor orbitals for NPHO

Donor *(i)*	Acceptor *(j)*	$E^{(2)}$/(kcal/mol)	$E(i)$−$E(j)$ (a.u.)	F(i,j) (a.u.)
LP (1) N_{12}	LP*(1) H_{10}	417.54	0.56	0.447
LP (2) O_{33}	LP*(1) H_{10}	145.56	0.62	0.296
πC_{15} - C_{16}	$\pi^* C_{22}$ - C_{31}	131.98	0.03	0.084
πC_{15} - C_{16}	$\pi^* C_{17}$ - C_{18}	130.67	0.02	0.078
πN_{12} - C_{30}	$\pi^* C_{28}$ - C_{29}	222.54	0.03	0.095

Donor *(i)*	Acceptor *(j)*	$E^{(2)}$/(kcal/mol)	*E(i)−E(j)* (a.u.)	*F*(i,j) (a.u.)
π^*N_{12} - C_{30}	π^*N_7 - C_8	171.99	0.02	0.072
π^*N_{12} - C_{30}	π^*C_1 - C_3	155.65	0.04	0.095
π^*N_7 - C_8	π^*C_{20} - O_{21}	83.59	0.05	0.095
LP (1) C_{27}	π^*C_{28} - C_{29}	71.79	0.13	0.106
LP (1) C_{27}	π^*C_1 - C_3	58.92	0.14	0.104
LP (3) O_5	π^*N_6 - O_9	137.60	0.11	0.114
πC_{28} - C_{29}	π^*N_6 - O_9	79.51	0.13	0.097
πC_{28} - C_{29}	LP (1) C_{27}	52.42	0.15	0.092
πC_1 - C_3	LP (1) C_{27}	54.65	0.14	0.093
πC_1 - C_3	π^*N_{12} - C_{30}	28.84	0.25	0.083
πN_6 - O_9	π^*C_{28} - C_{29}	41.63	0.16	0.096

3.7 Density of state (DOS) and orbital composition

In solid - state physics studies, the electronic energy density of states (DOS) of a system measures the number of electronic states that can be populated per unit energy interval. A material's DOS is an important parameter for identifying how each atom contributes to bonding, conductivity, magnetic order, optoelectronic properties, and other properties.[38, 39] The density of states (DOS) is the number of unique states allowed for electrons at a particular energy level, i.e. the number of electron states per unit volume per unit energy. The DOS plot was produced utilising Multiwfn to obtain additional information about the electron density distribution, which is shown in figure 3. The p orbital fraction dominates the electronic contribution to the total density of the state. The PDOS was displayed individually for the s, p, and d atomic orbitals, and the map shows that the occupied border molecular orbitals are predominantly given by the p-orbitals because most atoms have more electrons in their p-orbitals than their s-orbitals. Because neither NPHO nor CPHO contain electrons, their unoccupied d-orbital contributions are relatively small. Because they are derivatives of one other, NPHO and CPHO exhibit nearly identical TDOS curves; however, the contributions of the p orbitals of NPHO to the TDOS are slightly larger due to the nitrogen dioxide group in the molecule structure. This group's mesomeric influence is more chemically stable than CPHO and coincides with the results from the quantum descriptors. The plot also reveals that both compounds had an

energy gap that was lower than the fermi energy level. The hybridization between the *p* orbitals of the C, N, Br and Cl atoms and the *s* orbitals of H atoms accounts for the largest contributions to the distribution of the TDOS in both valence and conduction bands. The highest TDOS distribution is observed at the valence band and the energy bandgap of the highest occupied and lowest unoccupied molecular orbitals for NPHO and CPHO are observed between -0.80 a.u. to -0.31 a.u. and -0.80 a.u. to -0.29 a.u. respectively. The highest DOS is observed at -0.55 a.u. for both NPHO and CPHO.

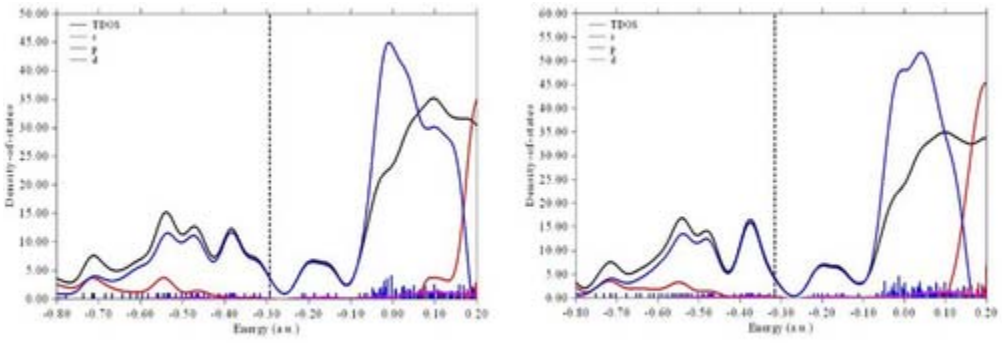

Figure 3
Open in figure viewerPowerPoint
The Total density of state plot of CPHO and NPHO

3.8 Molecular docking

When connecting a ligand to a target protein to produce a stable complex, molecular docking anticipates the preferred orientation of one molecule to another. Understanding of the preferential orientation, for example, can be employed to identify the binding affinity or strength of interaction between two molecules utilizing scoring functions.[40] The ligand chosen for this investigation was docked into the binding pocket of the receptor targets to demonstrate the compound's effectiveness as a prospective malaria treatment candidate. The docking interaction of the ligand and target proteins were assessed by the binding affinity which is the energy of inhibition of the receptor and drug molecule in addition to a variety of hydrogen bonds, hydrophobic interactions, polar and non-polar contacts as well as Van der Waals interactions between the receptor target and ligand molecule. Proteins selected for this study - **6J10** (Ciclopirox inhibits Hepatitis B Virus secretion by blocking capsid assembly) for Hepatitis B virus subtype adyw, 6T36 (Crystal structure of the PTPN3 PDZ domain bound to the HBV core protein C-terminal peptide) for Homo sapiens, Hepatitis B virus, 6MEI (Crystal structure of broadly neutralizing antibody HEPC3 in complex with Hepatitis C virus envelope glycoprotein E2 ectodomain) for Hepacivirus C, Homo sapiens, 4Z0X (Structure of Hepatitis C Virus Envelope glycoprotein E2 antigenic region 434-446 bound to the broadly neutralizing antibody HC26AM) for Homo sapiens, Hepacivirus C, were docked with synthesized azo compounds revealing certain spontaneous binding interaction as well as significant bond distance. The amino acid residues with conventional hydrogen bond interaction are crucial parameter for understanding many biochemical activities and biological processes.[41, 42]

From table 8, figure 4 and figures S2a-b (see supporting information), the ligands docked with the proteins revealed significant results indicating that both compounds have anti-hepatitis potentials. CPHO binding to 6J10 and 6T36 employed for hepatitis B revealed -6.4 and -5.1 kcal/mol as binding affinity respectively with a mean of -5.75 kcal/mol showing the conventional hydrogen bond interaction as the favourable interaction with the following amino acid residues and bond distance of TRP D:20(2.424Å), LEU D:140 (2.20 Å), PHE D:23 (5.50 Å), TRP D:30 (4.80 Å) and ASN A:55 (2.17 Å), ARG A:59 (2.62 Å), TYR A:50 (5.48 Å), TYR A:50 (4.51 Å) respectively, it can also be seen that

when interacted with the hepatitis C proteins (6MEI and 4Z0X), -5.5 and -6.3 kcal/mol were the observed binding affinities respectively with a mean of -5.9 kcal/mol. Showing the following amino acid residues and bond distance SER A:92 (2.46 Å), SER A:93 (2.73 Å), TRP A:90 (4.28 Å) and THR C:43 (3.93 Å), PHE C:44 (4.84 Å), PHE C:56 (5.23 Å), respectively. On the other hand, 6J10 and 6T36 when docked with NPHO their respective binding affinities were -6.3 and -5.2 kcal/mol with a mean of -5.75 kcal/mol outlining TRP D:10 (2.94 Å), SER D:10 (1.58 Å), TRP D:10 (3.02 Å), PHE D:12 (4.68 Å) and TYR A:50 (2.51 Å), ASN A:55 (2.2 Å), ARG A:59 (2.55 Å), TYR A:50 (5.49 Å) as the amino acid residues and bond distance respectively. NPHO had -6.6 and -6.6 kcal/mol as their binding affinity with a mean of -6.35 kcal/mol when docked with 6MEI and 4Z0X respectively. Showing their respective amino acid residues to be SER A:92 (2.26 Å), SER A:93 (2.50 Å), SER A:90 (2.30 Å), TRP A:50 (3.77 Å) and ASN C:44 (2.24 Å), ARG C:45 (2.42 Å). Entecavir and Ribavirin were the standard drugs employed for both hepatitis B and hepatitis C respectively. 6J10 and 6T36 when docked with entecavir which revealed -5.6 and -4.5 kcal/mol as their respective binding affinity with a mean of -5.05 elucidating TYR D:118 (5.82), PHE D:122 (5.30 Å), TRP D:102 (4.87 Å), PRO D:25 (5.27 Å) and PRO A:551 (4.98 Å), ARG A:596 (2.80 Å), ASN A:554 (2.09 Å), LYS A:552 (4.37 Å), ILE A:550 (4.84 Å) as the amino acid residues/bond distance respectively. On the other hand, -4.4 and -5.5 kcal/mol were the binding affinities predicted for 6MEI and 4Z0X when docked with NPHO respectively, indicating a mean binding affinity of -4.95 kcal/mol. With amino acid residues TYR A:31(1.98 Å), SER A:93 (2.50 Å), TRP A:90 (3.68 Å) and ARG C:455 (2.96 Å), GLY C:451 (2.56 Å), PRO C:619 (4.17 Å), TRP C:6176 for both proteins. This data however revealed that both CPHO and NPHO have great potential of treating hepatitis B when compared to the standard drug (Entecavir) reason been that CPHO had a higher and similar mean binding affinity of -5.75 kcal/mol when interacted with 6J10 and 6T36, it further indicates that, both compounds in a synergistic pattern will be a better therapy. On the contrary, ribavirin showed a low mean binding affinity of -4.95 kcal/mol when docked with 6MEI and 4T36 as CPHO and NPHO elucidated

Table 8. Molecular docking result of CPHO AND NPHO against four proteins and that of the standard drug

Properties	6J10	6T36	6MEI	4Z0X	Mean binding affinity
Binding affinity of CPHO	-6.4	-5.1	-5.5	-6.3	-5.83
Amino acid residue/Distance of CPHO	TRP D:20(2.424Å), LEU D:140(2.20Å), PHE D:23(5.50Å), TRP D:30(4.80Å)	ASN A:55(2.17Å), ARG A:59(2.62Å), TYR A:50(5.48Å), TYR A:50(4.51Å)	SER A:92 (2.46Å), SER A:93(2.73Å), TRP A:90(4.28Å)	THR C:43(3.93Å), PHE C:44(4.84Å), PHE C:56(5.23Å)	
Binding affinities of NPHO	-6.3	-5.2	-6.1	-6.6	-6.05

Properties	6J10	6T36	6MEI	4Z0X	Mean binding affinity
Amino acid residue/Distance of NPHO	TRP D:10(2.94Å), SER D:10(1.58Å), TRP D:10(3.02Å), PHE D:12(4.68Å),	TYR A:50(2.51Å), ASN A:55(2.2Å), ARG A:59(2.55Å), TYR A:50(5.49Å),	SER A:92(2.26Å), SER A:93(2.50Å), SER A:90(2.30Å), TRP A:50(3.77Å)	ASN C:44(2.24Å), ARG C:45(2.42Å)	
Binding affinity of Entecavir	-5.6	-4.5	-4.4	-5.5	5.00
Amino acid residue/Distance of Entecavir	TYR D:118(5.82Å), PHE D:122(5.30Å), TRP D:102(4.87Å), PRO D:25(5.27Å)	PRO A:551(4.98Å), ARG A:596(2.80Å), ASN A:554(2.09Å), LYS A:552(4.37Å), ILE A:550(4.84Å)	TYR A:31(1.98Å), SER A:93(2.50Å), TRP A:90(3.68Å)	ARG C:455(2.96Å), GLY C:451(2.56Å), PRO C:619(4.17Å), TRP C:6176	

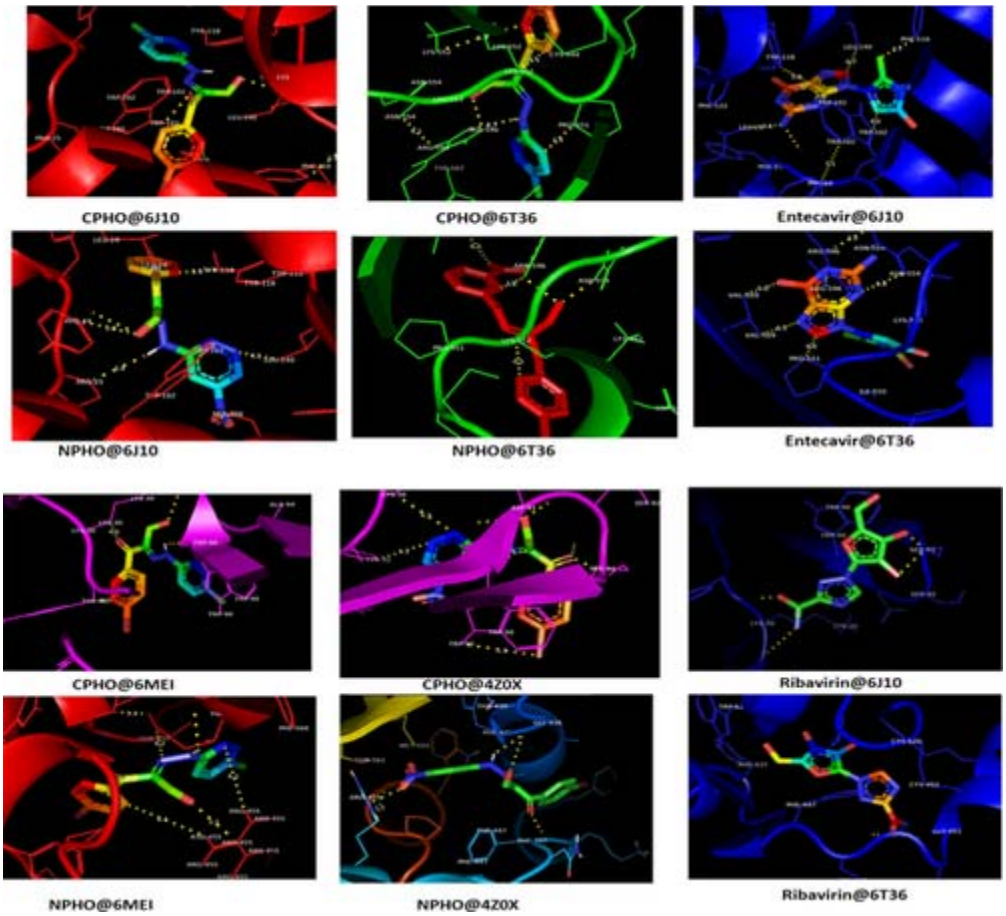

Figure 4

Open in figure viewerPowerPoint

Ligand-Protein Complex of CPHO, NPHO, Ribavirin and Entecavir with Receptor Protein respectively

higher mean binding affinity of -5.9 and -6.35 kcal/mol respectively.

4 CONCLUSIONS

Based on these findings, especially for the chemical hardness (*n*) and softness (S) confirms nitrophenyl derivatives of hydrazineylidene-3-oxopropanal (NPHO) to be more reactive compared to chlorophenyl derivatives of hydrazineylidene-3-oxopropanal (NPHO). The high NLO parameters observed are due to the high level of conjugation and electron delocalization within the molecule which agrees with the NBO stabilization energy values in NPHO, suggesting that NPHO has higher optical stability compared to CPHO. For the NBO analysis the high stabilization energies of NPHO indicates an intensive intermolecular interaction, electron delocalization and a high level of conjugation within the molecule compared to CPHO. FT-IR analysis indicated frequencies for CPHO slightly higher than those of NPHO due to the electron-withdrawing groups inductive effects of chlorine and bromine in CPHO, while the NO_2 group on NPHO allows for a more mesomeric effect on the molecule. In addition to the excellent ADME properties especially in the bioavailability based on the high percentage of intestinal absorption, both compounds CPHO and NPHO have great potential as antiviral agent for treatment hepatitis B and C when compared to the known drugs (Entecavir and ribavirin), and can be inferred that when administered as in a combination therapy both compound will have enhanced synergistic therapeutically merits.

Availability of data and material

All data are contained within the manuscript and manuscript supporting information document (ESI).

Competing Interests

All authors declare zero conflict of Interest.

Funding

This research did not receive funding from any source.

Authors Contribution

Hitler Louis: Project conceptualization, design, supervision, and administration. *Innocent Benjamin*: Writing, editing, analysis, and Manuscript draft. *Akaninyene D. Udoikono*: Writing, editing, analysis. *Tomsmith O. Unimuke*: Review and editing*. Ernest Agwamba and Eze F. Ahuekwe*: Writing, review, and editing.

Acknowledgements

The authors would like to acknowledge the center for high performance computing (CHPC), South Africa for providing computational resources for this research project. We also express appreciation to all those who have supported this work materially and intellectually.

Supporting Information
REFERENCES
Citing Literature

ISSN(Print) 2525-2321 ISSN(Online) 2572-8288

Vietnam Journal of CHEMISTRY

Volume 61, Number 1, February 2023

www.vjc.wiley-vch.de

WILEY-VCH

VIETNAM ACADEMY OF SCIENCE AND TECHNOLOGY

Volume61, Issue1

February 2023

Pages 109-125

- Figures

- References

- Related

- Information

Recommended

- Potential risk of HBV reactivation in patients with resolved HBV infection undergoing direct-acting antiviral treatment for HCV

  Eiichi Ogawa, Norihiro Furusyo, Masayuki Murata, Kazuhiro Toyoda, Takeo Hayashi, Kazuya Ura

  Liver International

- HBV reactivation in patients with HCV/HBV cirrhosis on treatment with direct-acting antivirals

  V. Calvaruso, D. Ferraro, A. Licata, M. G. Bavetta, S. Petta, F. Bronte, G. Colomba, A. Craxì, V. Di Marco

  Journal of Viral Hepatitis

- Theoretical investigation of the molecular structure, vibrational spectra, and molecular docking of tramadol using density functional theory

  Yunusa Umar, Sahar Abdalla, SK Manirul Haque, Guillermo Salgado Moran, Abdurrahman Ishaq, Wilson Cardona Villada, Jorge Dagnino Leone, Marta Bunster

  Journal of the Chinese Chemical Society

- Synthesis, characterization, DFT studies, and molecular modeling of hydrazinelidene-3-oxo-3-(*p*-olyl) propanal derivatives as potential candidate for Hepatitis B and C treatment

  Hitler Louis, Thank God C. Egemonye, Henry O. Edet, Ernest C. Agwamba, Tomsmith O. Unimuke, Adedapo S. Adeyinka

  Vietnam Journal of Chemistry

- Virtual Screening, Molecular Docking, and DFT Studies of Some Thiazolidine-2,4-diones as Potential PIM-1 Kinase Inhibitors

  Vivek Asati, Santosh S. Thakur, Neeraj Upmanyu, Sanjay K. Bharti

  ChemistrySelect

  Download PDF
  Back

Additional links

ABOUT WILEY ONLINE LIBRARY

- Privacy Policy
- Terms of Use
- About Cookies
- Manage Cookies
- Accessibility
- Wiley Research DE&I Statement and Publishing Policies
- Developing World Access

HELP & SUPPORT

- Contact Us
- Training and Support
- DMCA & Reporting Piracy

OPPORTUNITIES

- Subscription Agents
- Advertisers & Corporate Partners

CONNECT WITH WILEY

- The Wiley Network
- Wiley Press Room